Brain Stimulation 18 (2025) 1750–1763

Contents lists available at ScienceDirect

Brain Stimulation

journal homepage: www.journals.elsevier.com/brain-stimulation

Multidimensional Motor Evoked Potentials (MultiMEP): Digging up buried information from single trials

Francesca Genovese [a,b,1], Elena Mussini [a,b,1], Agnese Zazio [c], Fabio Beltrami [a], Marta Bortoletto [d], Luigi Cattaneo [e], Paolo Rota [e], Francesco Negro [f], Martina Fanghella [a,b], Corrado Sinigaglia [a,b], Guido Barchiesi [a,b,*]

[a] Department of Philosophy, University of Milan, via Festa Del Perdono, 7, Milan, 20122, Italy
[b] Cognition in Action (CIA) Unit, PHILAB, University of Milan, Via Santa Sofia, 9, 20122, Italy
[c] Neurophysiology Lab, IRCCS Istituto Centro San Giovanni di Dio Fatebenefratelli, Via Pilastroni,4, 25125, Brescia, Italy
[d] Molecular Mind Laboratory, IMT School for Advanced Studies Lucca, Piazza S.Francesco, 19, 55100, Lucca, Italy
[e] Center for Mind and Brain Sciences, CIMeC, University of Trento, Corso Bettini,31, Rovereto, 38068, Italy
[f] Department of Clinical and Experimental Sciences, University of Brescia, Viale Europa, 11, 25123, Brescia, Italy

ARTICLE INFO

Keywords:
Motor evoked potentials (MEP)
Transcranial magnetic stimulation (TMS)
Multivoxel pattern analysis (MVPA)
Single-trial
Motor imagery
Decoding
Cross-classification

ABSTRACT

Background: To investigate covert motor processes, transcranial magnetic stimulation (TMS) studies often use motor-evoked potentials (MEPs) as a proxy for inferring the state of motor representations. Typically, these studies test motor representations of actions that can be produced by the isolated contraction of one muscle, limiting both the number of recorded muscles and the complexity of tested actions. Furthermore, univariate analyses treat MEPs from different muscles as independent, overlooking potentially meaningful intermuscular relationships encoded in MEPs amplitude patterns at the single-trial level.

Objective: We addressed these limitations by adopting a decoding approach to MEPs analogous to multivoxel pattern analysis in neuroimaging.

Methods: Using our novel *Multidimensional Motor Evoked Potentials (MultiMEP)* approach, we tested 22 participants by applying a decoding analysis to MEPs recorded from 24 electrodes during motor imagery of three complex hand actions.

Additionally, to test whether imagery and action production shared common representations, we conducted an exploratory cross-classification analysis by training a classifier on one domain (MultiMEP evoked during motor imagery or action execution electromyographic patterns) and testing it on the other.

Results: Imagined actions were classified, based on MultiMEP patterns, with an accuracy of 74 %.

The cross-classification analysis yielded above-chance accuracies of 54 % (execution-to-imagery) and 71 % (imagery-to-execution).

Conclusions: This proof-of-principle study demonstrates that MEPs encode richer information than previously assumed both at single-subject and at single-trial levels.

Our results suggest that MultiMEP decoding represents a first step toward a paradigm shift in studying motor processes with TMS, much like multivoxel pattern analysis revolutionized the way the brain-cognition relationship has been studied through neuroimaging.

1. Introduction

Research on covert motor processes such as motor imagery [1–4], action observation [5–10], motor preparation [11–17], inhibition [18–20] or other similar covert activities [21,22] often employs suprathreshold transcranial magnetic stimulation (TMS) of the motor cortex to elicit motor evoked potentials (MEPs) from muscles associated with the processed actions [23].

For example, in a widely employed experimental design, researchers examine motor representations underlying covert processing of index and little finger abduction, which depend on the isolated first dorsal interosseous (FDI) and abductor digiti minimi (ADM) contraction,

* Corresponding author. Department of Philosophy, Università degli Studi di Milano, Via Festa del Perdono 7, 20122, Milano, Italy.
E-mail address: guido.barchiesi@unimi.it (G. Barchiesi).
[1] These authors equally contributed to the research reported in the present work

https://doi.org/10.1016/j.brs.2025.09.001
Received 28 March 2025; Received in revised form 25 July 2025; Accepted 2 September 2025
Available online 4 September 2025

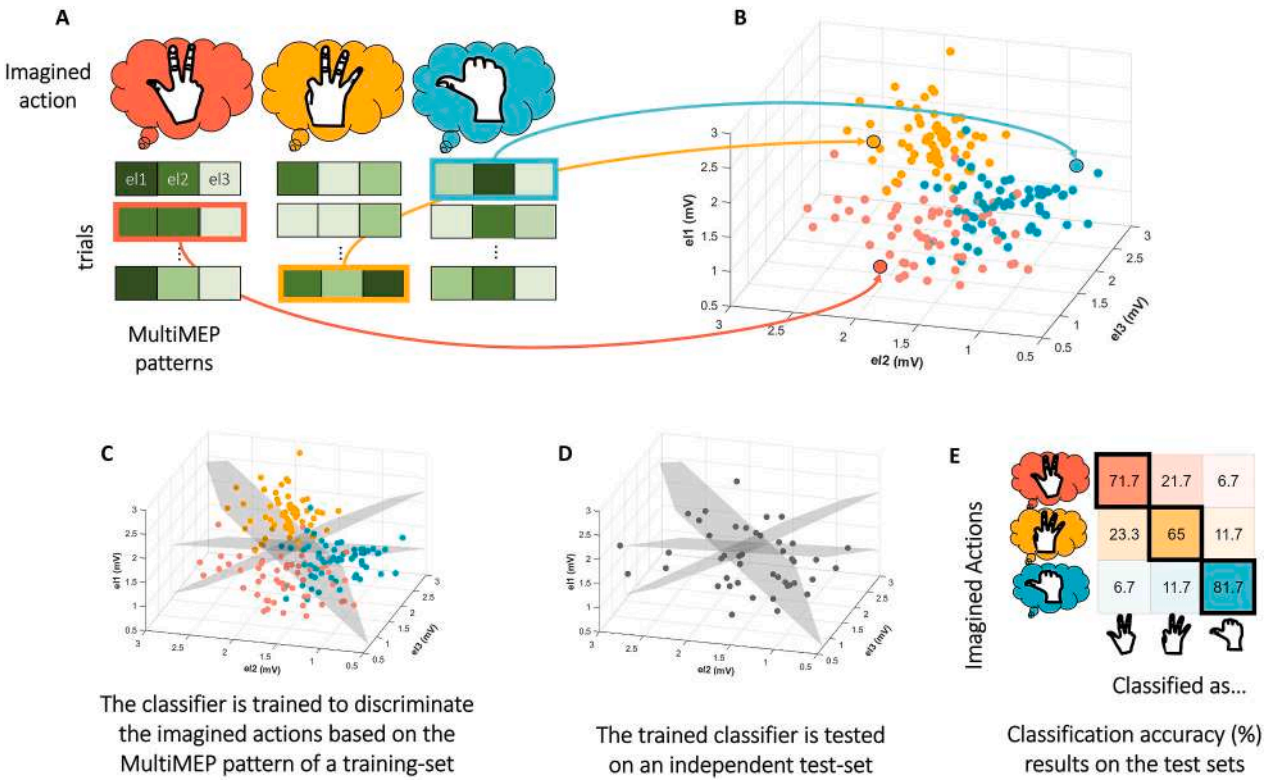

Fig. 1. MultiMEP decoding rationale

A. MultiMEP decoding approach: White-to-green arrays represent a vector of the MEPs amplitudes recorded from each electrode (el1, el2, el3, for visualization purposes, only 3 electrodes are represented) during the imagery of complex actions (i.e., actions that, if produced, would involve the contraction of several muscles).

B. A 3D representation of an ideal MultiMEP-space where each dot represents a single trial MultiMEP pattern; the dot's position in the MultiMEP-space is determined by the amplitude of MEPs recorded on each electrode. The dot color represents the action imagined in a specific trial.

C. Using a supervised learning approach, the classifier is trained to estimate hyperplanes that best distinguish between imagined actions based on MultiMEP patterns from a so-called "training-set" of trials.

D. The estimated hyperplanes are employed to test their classification accuracy on an independent set of trials called test-set.

E. A confusion matrix is computed: each row corresponds to the totality of trials where a specific action is imaged, while the columns partition the trials according to the classifier predictions. The cells on the main diagonal correspond to the correct classification percentages for each action imagined. A perfect classification would then be represented as 100 % on the main diagonal cells and 0 % on the off-diagonal cells.

respectively. The design follows a 2 (actions) × 2 (muscles) structure, with MEP amplitudes as the dependent variable. Amplitudes are averaged within each condition, and an interaction between factors is analyzed. An increase of FDI MEPs when observing or imagining index finger abduction compared to little finger abduction allows to infer that the index finger abduction motor representation is facilitated (and vice versa for ADM in relation to little finger abduction processing) [5,8,24–29].

Most of these studies share methodological features that simplify testing but at the cost of limiting the information extracted from MEPs, which reduces the possibility of a thorough understanding of how motor content is represented during covert processes.

They implicitly adopt a "one-muscle one-action" (1m1a) approach assuming that each studied action depends solely on the isolated contraction of one of the recorded muscles. This limits the range of testable actions, as identifying additional one-to-one muscle-action pairs becomes increasingly challenging, and it reduces the ecological validity of the results as the studied actions are often single-joint movements rarely occurring in isolation in real-life.[2] Additionally, 1m1a studies average MEP amplitudes within design cells, improving the signal-to-noise ratio but discarding valuable single-trial information. Lastly, the adopted univariate analyses treat the recorded muscles as independent levels of a factor, disregarding inter-muscle relationships and thus losing valuable information. As a result, much of the potential insights from single-trial MEP data remains substantially unexplored.

Here, we introduce Multidimensional Motor Evoked Potentials (MultiMEP) to address these limitations. Inspired by Multivoxel Pattern Analysis (MVPA) [30–33], which classifies condition-specific information from voxels activity patterns, in the MultiMEP decoding framework we aim at discriminating covertly processed actions based on the multidimensional pattern of MEPs recorded from different muscles, rather than treating them as independent units of analysis. Just as MVPA enhances information discrimination in neuroimaging studies, we expected a similar advantage in MultiMEP, given that different locations on an effector are differentially influenced by distinct upstream corticospinal input.

In a proof-of-concept experiment, we recorded MEPs from 24 forearm electrodes while participants imagined three complex hand actions that, if produced, would involve the contraction of multiple muscles. We then used supervised learning classification to train an algorithm to distinguish between imagined actions based on MultiMEP patterns. The classifier estimates hyperplanes in a multidimensional space to separate activity patterns associated with each action. Hyperplanes decoding generalizability was tested on new trials, with classification accuracy reflecting their ability to decode imagined actions from MultiMEP amplitude patterns (Fig. 1).

This decoding approach overcomes the information limitations

[2] This problem has been mitigated by a minority of studies using inertial sensors [81–84] or ultrasound tissue Doppler imaging [85] to investigate more naturalistic motor representations.

imposed by the 1m1a strategy by enabling the study of complex actions, leveraging activity patterns across multiple electrodes, and fully exploiting relational information between MEPs. Once trained, the classifier model categorizes imagined actions based on single-subject and single-trial MultiMEP data.

In an exploratory analysis, we demonstrated that MultiMEP can support inferences similar to 1m1a experiments within a multidimensional decoding framework. We tested a classic claim, derived from early 1m1a studies, supporting the idea that motor imagery and action production share motor representations [1,34,35]. To test this we also extracted contraction patterns and trained two classifiers in two directions: one has been trained on the contraction domain and tested on the MultiMEPs evoked during imagery, while the other has been trained on MultiMEPs and tested on contraction patterns. If motor representations are shared, cross-classification pattern discriminability should exceed chance, mirroring classical 1m1a findings. Eventually, we conducted a cross-subjects classification analysis to explore the similarity between decoding spaces across participants, and an electrode selection analysis, to explore the contribution of different arm areas to the classification outcome.

2. Methods

2.1. Participants

Twenty-five right-handed [36] participants (15 females, mean age: 22.6 years), took part in the experimental session. Ad-hoc exclusion criteria corresponded to the safety criteria for TMS [37,38]. For this purpose, all potential participants were screened for neurological and psychiatric conditions using a TMS exclusion criteria questionnaire prior to participation. Of the 25 individuals initially recruited, 22 were included in the final analysis: two participants were excluded due to difficulty in relaxing the target muscles, and one withdrew due to subjective discomfort. No major adverse effects were reported by any participant. The study was approved by the ethical committee of the University of Milan ("MultiMEP: Potenziali Evocati Motori Multidimensionali") and conducted in accordance with the revised Helsinki Declaration [39], with written informed consent obtained from all participants.

We based our sample estimation around a classical motor imagery task employed in Rossi et al., 1998 [34]. There, we calculated the effect size of their outcomes resulting in a Cohen's d = 1.43. We then calculated, using the same effect-size, the sample size for a paired-sample and a one-sample Wilcoxon-test (two-tails), with alpha = 0.05 and power = 0.8. We obtained a sample of 5 and 7 participants. In order to increase the generalizability of the results we arbitrarily incremented the participants number to 25.

2.2. Procedure

The entire procedure consisted of the electrode grid montage, hotspot and intensity hunting procedure, instructions, practice, and finally, the experimental block. The whole session lasted approximately 2–2.5 h.

2.2.1. Electrodes grid montage

Experimenters began electrode placement by scrubbing the skin of the right forearm with scrubbing paste [40]. Electromyographic (EMG) recordings were obtained using 24 passive sintered Ag/AgCl ring electrodes (model: B10, length: 150 cm, EasyCap GmbH, Germany) arranged in four strips of six electrodes each, spaced 2.5 cm apart. On the dorsal surface of the forearm, one strip was aligned along the radial side, with the gap between the fourth and fifth electrodes positioned midway down the forearm, while a second strip was placed medially with a 1.25 cm posterior shift; a similar setup was used on the volar surface, with the third strip aligned along the ulnar side and the fourth anteriorly shifted (Fig. 2). The advantage of a grid of evenly distributed electrodes covering a substantial portion of the forearm consists in reducing potential a-priori electrode placement problem [41]. Disposable ground and reference electrodes were positioned on the proximal volar or dorsal forearm, and the electrode grid was secured with adhesive tape. Conductive gel was applied inside each ring via syringe to achieve conductance levels below 40 kΩ.

Monopolar recordings of EMG were achieved by connecting the electrodes to 24 pins on a BePlusPro Advanced amplifier (EBNeuro, Italy), with data sampled at 4096 Hz. A 10 Hz high-pass filter was applied solely for visualization purposes, not affecting the recorded

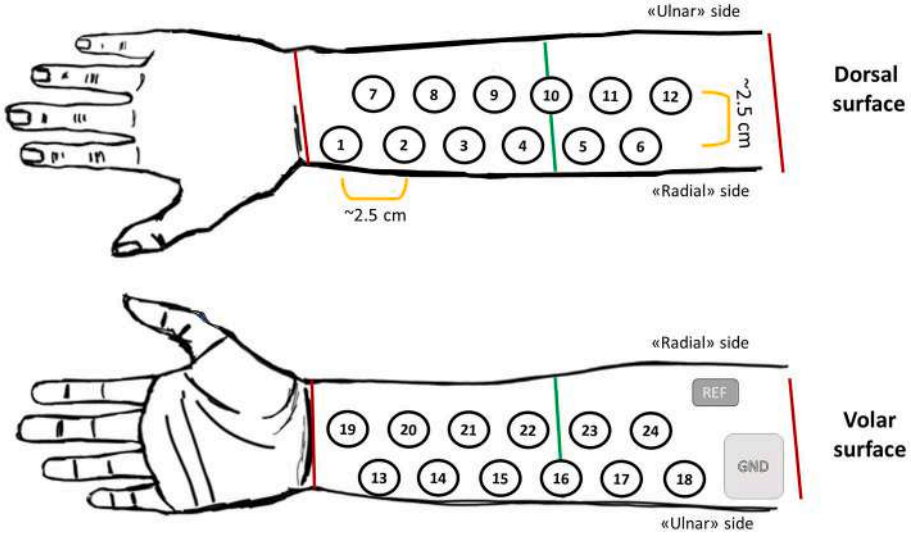

Fig. 2. Electrode Grid montage
Four strips, each containing six passive sintered ring electrodes (typically used for electroencephalographic recordings) spaced 2.5 cm apart (24 electrodes total), were used for electromyographic recordings. On the dorsal surface of the forearm, the first strip was aligned along and above the radial bone ("radial" side), with the gap between the fourth and fifth electrode positioned midway down the forearm (green lines), measured from the styloid process to the lateral epicondyle (red lines). The second strip was placed 2.5 cm medially and posteriorly shifted to approximately 1.25 cm. The same arrangement was applied to the volar surface of the forearm, except the third strip was aligned along the "ulnar" side, and the second strip was shifted 1.25 cm forward. Ground and reference electrodes were disposable electrodes, typically placed on the proximal area of the forearm, depending on available space.

data.

To increase the spatial specificity, we computed, for visualization purposes, bipolar derivations of the electrodes by taking the difference between pairs of filtered monopolar recordings [42,43] along the longitudinal dimension of the forearm for each of the four strips (1–2 to 5–6, 7–8 to 11–12, 13–14 to 17–18, 19–20 to 23–24) and transversely from the dorsal surface (1–7, 6–12, 13–19, 18-24), for a total of 24 bipolar derivations.

To check the signal during the experimental session, we took advantage of the Lab Streaming Layer functions (https://labstreaminglayer.org/#/, [44]), extracting the recorded signal stream from the amplifier and building our own customized "MultiMEP Viewer" which was displayed on the amplifier-PC (MATLAB2021b, MathWorks). The Viewer was composed of two windows: the "continuous stream window," where the continuous native monopolar data streams were plotted, and the "multi-epochs window", where MEPs calculated on the 24 bipolar derivations, were displayed between −150 and 400 ms from the TMS trigger, and whose peak-to-peak amplitude was automatically calculated between 15 ms and 65 ms from the TMS trigger.

2.2.2. TMS

Biphasic TMS pulses were delivered via a 70-mm butterfly coil connected to an STM9000 stimulator (inducing anterior-to-posterior currents) and guided by the NETBRAIN9000 neuronavigation system (EBNeuro, Italy). Participants' heads and the coil were coregistered to a standard 3D MNI brain mesh.

Seated on an armless chair, participants rested their heads on a chin rest while their right arm remained relaxed, hanging naturally with the hand pointing downward. This posture, maintained throughout intensity hunting procedure and the experiment, minimized pre-TMS muscle contractions while allowing unobstructed execution of the displayed actions. If uncomfortable, participants could lean back to further reduce background muscle activity.

To identify the 'MultiMEP hotspot', we performed a grid-search procedure over the left hemisphere, holding the coil tangential to the scalp at an angle of ~ 45° relative to the anterior–posterior axis. Stimulator intensity was varied in steps of 5% of the maximum output, starting from 20%. The hotspot was defined as the scalp location capable of evoking, at rest, MEPs with amplitudes peak-to-peak ≥ 50 μV in at least 18 of 24 displayed bipolar derivations in five consecutive single pulses (MEPs peaks search time-window: 15–65 ms). The lowest intensity meeting this criterion was used as the stimulation intensity for the experimental session (average stimulation intensity: 56.8 % ± 8 %). The rationale for the intensity-hunting strategy has been described in more detail in the Supplementary Materials.

2.2.3. Stimuli, task, and Trial Structure

The stimuli consisted of drawings of a right hand representing three different gestures ("three," "ok," and "hitchhiking (hh)"). The fingers pointed downwards to resemble the participant's hand position (Fig. 3).

Participants performed a 'Move-then-Imagine' task: after a Go-signal, they executed the action displayed on the screen as quickly as possible, then relaxed, and finally engaged in sensorimotor imagery of the same action: "… imagine the action you have just executed by recalling the muscular tension, the sensation on the skin and within the joints, that the production of that action evoked, but in doing so, do not contract the muscles." [35,45]. During the imagery phase a single TMS pulse was delivered on the MultiMEP hotspot (Fig. 3). A familiarization phase was conducted before the onset of the experimental block (Supplementary Materials).

Each trial started with a blank screen for 1 s, followed by the presentation of one right-hand action drawing. After 1 s, a "Go-signal" high-pitch sound was played through speakers on each side of the presentation PC monitor. After participants had executed the depicted action, they were required to keep the muscular contraction until, after 1 s, a low-pitched sound was played along with a visually presented "stop" label (1 s), commanding complete muscular relaxation. A feedback screen followed for 0.5 s. If participants anticipated the execution of the action, a red "already contracted" label was displayed as feedback; if participants produced the action after the deadline, a red "no response" label was shown instead. If they correctly produced the action within the response window, their reaction time (RT, deadline < 350 ms from the Go-signal) was displayed in green (see Supplementary Materials for RT calculation). After the feedback, a 1 s blank screen was presented; next, the same drawing shown at the onset of the trial was presented along with a blue label "*imagine to perform the drawn gesture*"; after 2 s, a TMS pulse was delivered on the participant's MultiMEP hotspot. Following the TMS pulse, participants were asked to stop imaging and prepare for the next trial. If pre-TMS muscular contraction was detected, which was defined as a peak-to-peak amplitude greater than 75 μV in the 50 ms before the TMS pulse in at least one of the bipolar derivations, a red

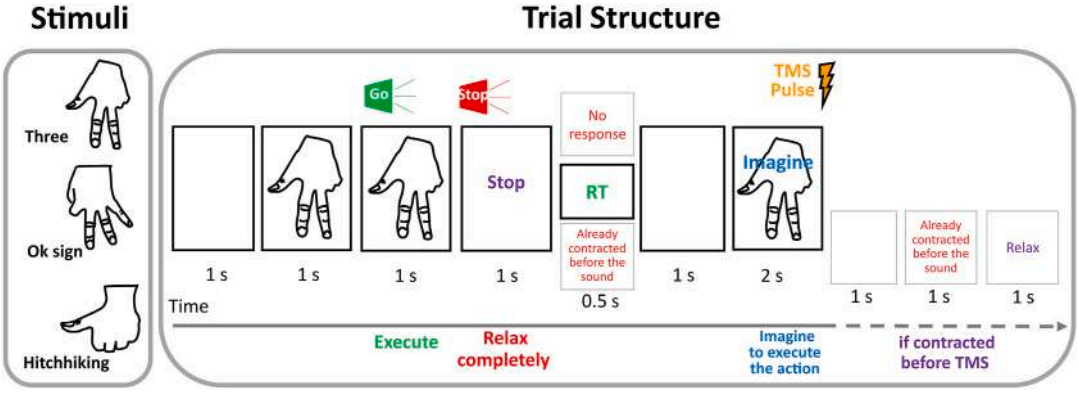

Fig. 3. Stimuli and Trial Structure

Stimuli. Action drawings presented during the experiment: a "three" sign with thumb, index, and middle fingers extended and ring and little fingers flexed; an "ok" sign with middle, ring, and little fingers extended while the tips of the index touched the thumb, and a "hitchhiking (hh)" gesture with the thumb extended, and all the remaining fingers flexed. The downward orientation of the drawings matched the participants' hand position.

Trial structure. Each trial started with an action drawing. After a second, a Go-signal commanded to execute the drawn action as fast as possible and keep the contraction until the stop sound signal, which instructed the muscles to relax completely. Next, feedback was displayed relative to the performance. After a 1 s blank screen, the same action drawing and an "imagine" label were presented again. After 2 s, a TMS was delivered on the MultiMEP hotspot. If pre-stimulus contraction was detected (defined as > 75 μV in the 50 ms before the TMS pulse in at least one of the visualized bipolar derivations), feedback was displayed, followed by a relax label.

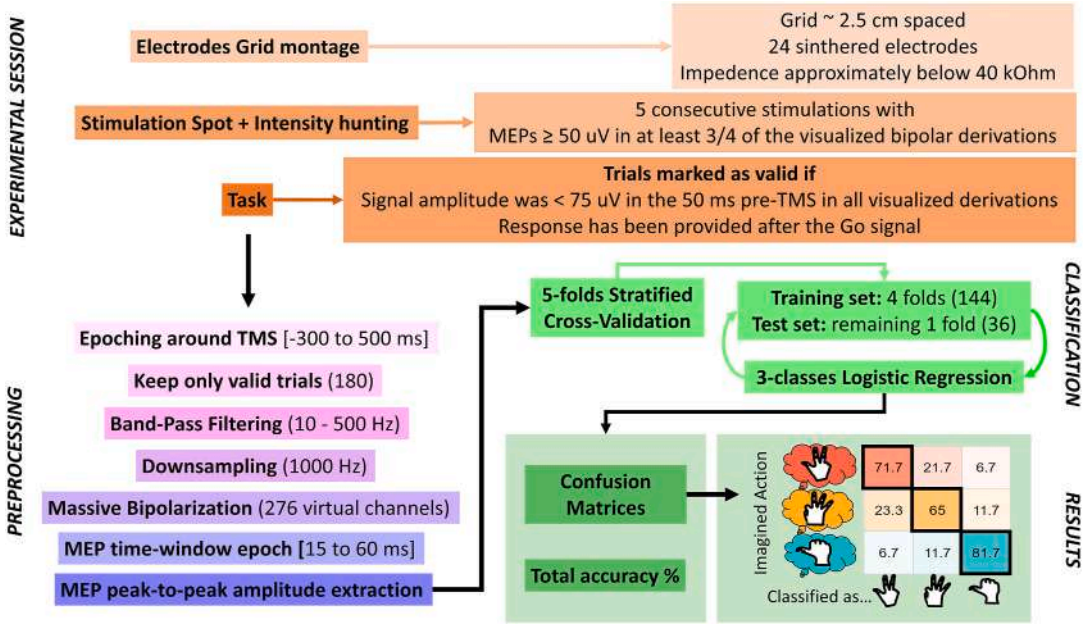

Fig. 4. Main experimental steps: montage (shades of orange), preprocessing (shades of purple), classification and results (shades of green).

"already contracted" label was displayed for 1 s, followed by a "relax" label lasting 1 s. In the latter case or in the case no response was provided after the Go-signal, the trial was marked as non-valid and rescheduled randomly (Fig. 4 Experimental Session panel). This strategy allowed us to record 180 clean trials, 60 trials for each of the three imagined actions (see Supplementary Materials Table S1 for a summary of rescheduled trials number).

The action production during the first part of each trial had the double purpose of providing a fresh "haptic-proprioceptive" model that was putatively easier to retrieve from memory during the motor imagery part of the trials [46,47] and keeping participants engaged, preventing them from getting bored or falling asleep.

3. Analyses

3.1. MultiMEP classification

3.1.1. Data preprocessing

We employed a decoding approach (Fig. 1) to discriminate the imaged actions based on the MEP amplitude patterns. All analyses relied on custom scripts developed in MATLAB (including functions from the Fieldtrip toolbox [48]), Python (including Scikit-learn libraries for the classification algorithms [49]), and R [50] (including ggplot functions [51]).

Each participant's dataset has been epoched around the TMS trigger between −300 and 500 ms. Trials contaminated by pre-TMS contractions, as defined in the "Stimuli, Task, and Trial Structure" paragraph, were removed, ensuring that exactly 60 valid trials were analyzed for each imagined action.

Forward 4th order Butterworth 10 Hz high-pass and 500 Hz low-pass filters have been applied to padded epochs. Next, the filtered epochs have been downsampled to 1000 Hz to reduce the computational load.

To fully exploit the spatial information embedded in the EMG signals, we implemented a procedure we refer to as "massive bipolarization". This involved computing all possible bipolar derivations by subtracting the signal of one electrode from another for every unique pair of the 24 monopolar channels. Mathematically, this corresponds to all pairwise combinations of the 24 channels, resulting in 276 bipolar derivations (virtual channels). Thus, each virtual channel reflects the voltage difference between two monopolar electrodes.

For each virtual channel, we calculated the peak-to-peak amplitude of the MEPs within the 15–60 ms time window after the TMS pulse.

Thus, a matrix of MEP amplitudes (MultiMEP matrix) constituted by 180 trials (rows) × 276 MEPs virtual channels (columns) has been computed, along with a vector containing the imagined action labels for each trial (Fig. 4 Preprocessing panel).

3.1.2. Classification

The MultiMEP matrix was classified using 3-class logistic regression within a 5-fold stratified cross-validation algorithm: each dataset was randomly split into five equal parts (folds) ensuring that each fold maintained equal proportions of trials belonging to the three classes.

The logistic regression model was trained on four folds (training-set) and tested on the remaining one (test-set), repeating this process five times so that each fold serves as the test-set once (Fig. 4 Classification panel). At the onset of each cross-validation cycle the training-set was z-scored, and the same transformation was applied to the test-set. The model performance was averaged across all five runs. No hyperparameter tuning was performed.

We then computed a confusion matrix for each participant: for each action imagined (rows) we calculated the classifier prediction percentages. Eventually, a total accuracy metric was computed indicating the percentage of correctly classified trials. (Fig. 4 Results panel).

Three tests were performed:

Single subject total accuracy: We tested whether MultiMEP contained sufficient information to classify imagery content above chance at the single-subject level. To determine statistical significance, we followed the approach of Combrisson & Jerbi [52], who underscore that the commonly assumed 33.3 % chance level (for three classes) applies only with an infinite number of trials. Given that classification under the null hypothesis follows a cumulative binomial distribution, the probability of achieving 38.9 %, 41.6 %, or 44.4 % classification accuracy in our experiment (3 classes, 60 trials per class) corresponded to p-values <0.05, <0.01, and <0.001, respectively.

Group total accuracy: At the sample level, we tested if total classification accuracies were, on average, above the theoretical chance level by performing a non-parametric Wilcoxon test on total accuracies against 33.3 %.

Classification Bias: To test if the total accuracy was inflated by a particularly easy-to-classify action, we extracted the accuracies

corresponding to the on-diagonal elements of the confusion matrices for each participant. This resulted in 22 accuracy percentages for each imagined action, which underwent a Friedman test ($p < 0.05$).

3.2. Exploratory analysis: cross-classification between contraction and imagery patterns

In this exploratory analysis, we applied a MultiMEP decoding approach to test the claim, derived from classic 1m1a motor imagery works, that action production and motor imagery share common motor representations. To this aim, we took advantage of the contraction patterns (henceforth "MultiEMG") collected when participants produced the observed actions. After checking that MultiEMG patterns were well discriminable, we performed two cross-classifications in two directions, by training the classifier on MultiMEP and testing it on MultiEMG (MultiMEP-to-MultiEMG), and vice versa (MultiEMG-to-MulitEMG).

3.2.1. MultiEMG data preprocessing

Preprocessing of MultiEMG patterns followed a procedure very similar to the one employed to obtain MultiMEP: the recorded EMG data were epoched between −300 and 1000 ms from the Go-signal. EMG traces from valid trials were filtered, downsampled, and massively bipolarized. Differently from MultiMEP analysis, a root-mean square value was calculated for each trial and each virtual channel, considering a time window ranging from the earliest contraction onset (see Supplementary Materials) until the following 200 ms. Eventually, a 180 trials x 276 matrix was computed along with the labels for each trial.

3.2.2. Sanity check: MultiEMG classification

To test if the executed actions were discriminable from MultiEMG patterns, we applied the MultiMEP pipeline analysis to the MultiEMG data.

3.2.3. Cross-classification between contraction and imagery patterns: data pre-processing

A crucial preprocessing step was aligning the multidimensional spaces of MultiEMG and MultiMEP, as their amplitudes are not directly comparable. TMS-induced MEPs exhibit muscle-specific biases (TMS-bias pattern) influenced by individual brain-skull anatomy, unlike voluntary contractions recorded in MultiEMG. Assuming a simple additive interaction, MultiMEPs during imagery reflect the combination of both the TMS-bias and imagery-specific patterns. Even if corticospinal activity during imagery mirrored execution, the TMS-bias would shift the position of the MultiMEP patterns within multidimensional space. To correct for this, we z-scored both datasets along the virtual channel dimension, reducing the TMS-bias while preserving trial-specific activity patterns and "within-electrode" relationships (Fig. 5).

3.2.4. Cross-classification between contraction and imagery patterns: classification

After the "within-electrode" standardization, we conducted two cross-classifications using a modified 5-fold cross-validation algorithm. In this approach, the training folds were drawn from one domain (MultiEMG or MultiMEP), while the test fold came from the other (MultiMEP or MultiEMG, respectively). This ensured that, in each fold, the trials used to fit the classification model remained entirely independent from those in the test set.

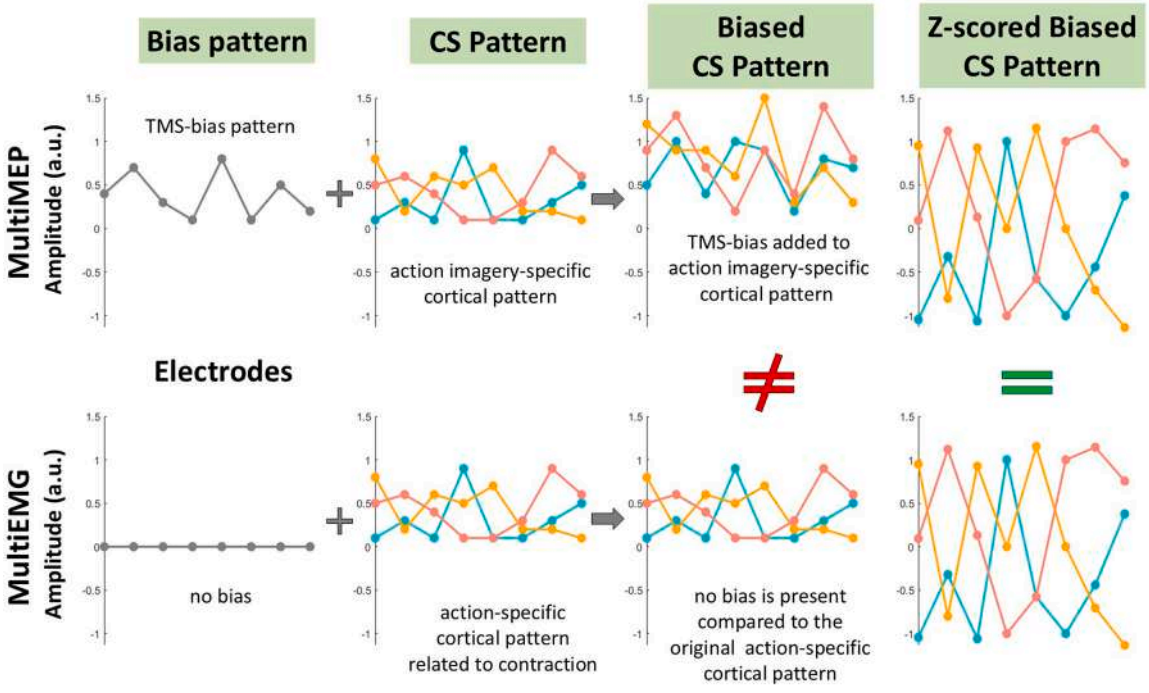

Fig. 5. Schematic Representation of the TMS-bias Reduction by z-scoring along the Electrode dimension

Bias Pattern. Two hypothetical datasets (MultiMEP and MultiEMG) each composed of three different motor representations (different colors) are displayed as rows. Each plot shows eight hypothetical electrodes on the x-axis and amplitude (arbitrary units) on the y-axis. The first plot of the two rows represents the influence of the TMS-bias on electrodes amplitude: the bias affects MultiMEP only.

CS Pattern. Hypothetical corticospinal representation (CS) of the three motor representations, assumed to be identical between the two datasets by hypothesis.

Biased CS Pattern. Interaction between TMS-bias and corticospinal representation: the patterns of the three motor representations are no longer identical between the two datasets, as those in MultiMEP are influenced by the TMS-bias.

Z-scored Biased CS Pattern. z-scoring "within-electrode" brings back the similarity between the corresponding motor representations of the two datasets. Note that, compared to the CS Pattern, the relationship between conditions does not change within electrodes.

3.3. Exploratory analysis: cross-subjects MultiMEP classification

To assess the degree of similarity of decoding spaces across participants, we implemented the following pipeline: the MultiMEP dataset was first z-scored separately for each participant. Then, a logistic regression model was trained on each participant's data (180 trials; 60 per action class) and tested on the data from each remaining participant. This procedure was repeated for each participant, resulting in 21 cross-subjects classification outcomes per individual. These were then averaged to produce a participant-level metric reflecting the similarity between their MultiMEP-derived decoding space and that of others. To determine whether this cross-subjects similarity exceeded chance level (33 %), we compared each participant's average classification accuracy to chance using a Wilcoxon signed-rank test.

3.4. Exploratory analysis: MultiMEP classification accuracy for electrode grid subdivisions

In the present experiment, electromyographic activity was recorded from 24 surface electrodes arranged over the forearm. However, it is possible that not all 24 electrodes are necessary to achieve optimal classification accuracy. Furthermore, certain forearm regions may contribute more consistently to discriminating imagined actions than others.

To investigate these possibilities, we assessed classification performance using subsets of electrodes defined by spatial subdivisions: four Quadrants, four Half-Grid regions, and the Whole Grid.

Quadrants subdivisions: The grid was divided into four anatomical quadrants: dorsal anterior (electrodes 1, 2, 3, 7, 8, 9), dorsal posterior (4, 5, 6, 10, 11, 12), volar anterior (13, 14, 15, 19, 20, 21), and volar posterior (15, 16, 17, 22, 23, 24) aspects of the forearm.

Half-Grid subdivisions: Two orthogonal subdivisions were used: one separating the dorsal (electrodes 1–12) and volar (13–24) aspects, and another separating the anterior (1, 2, 3, 7, 8, 9, 13, 14, 15, 19, 20, 21) and posterior (4, 5, 6, 10, 11, 12, 15, 16, 17, 22, 23, 24) aspects of the forearm.

Whole Grid: All 24 electrodes (1–24) were included in the analysis.

For each spatial subdivision, we computed all possible bipolar derivations resulting in: 15 virtual channels for each Quadrant, 66 for each Half-Grid region, and 276 for the Whole Grid. This resulted in four 180 × 15 matrices (one per quadrant), four 180 × 66 matrices (one per Half-Grid), and one 180 × 276 matrix (Whole Grid). These matrices were entered into a classification procedure identical to that used for the MultiMEP-to-MultiMEP analysis.

To statistically assess differences in classification performance across the nine spatial configurations, we first applied a Friedman test. Pairwise comparisons between subdivisions were then conducted using paired Wilcoxon signed-rank tests, with Benjamini-Yekutieli correction applied to control for multiple comparisons.

4. Results

4.1. MultiMEP classification

Single subject's total accuracy: We tested how well single participants' total accuracy classification departed from an empirical chance level:

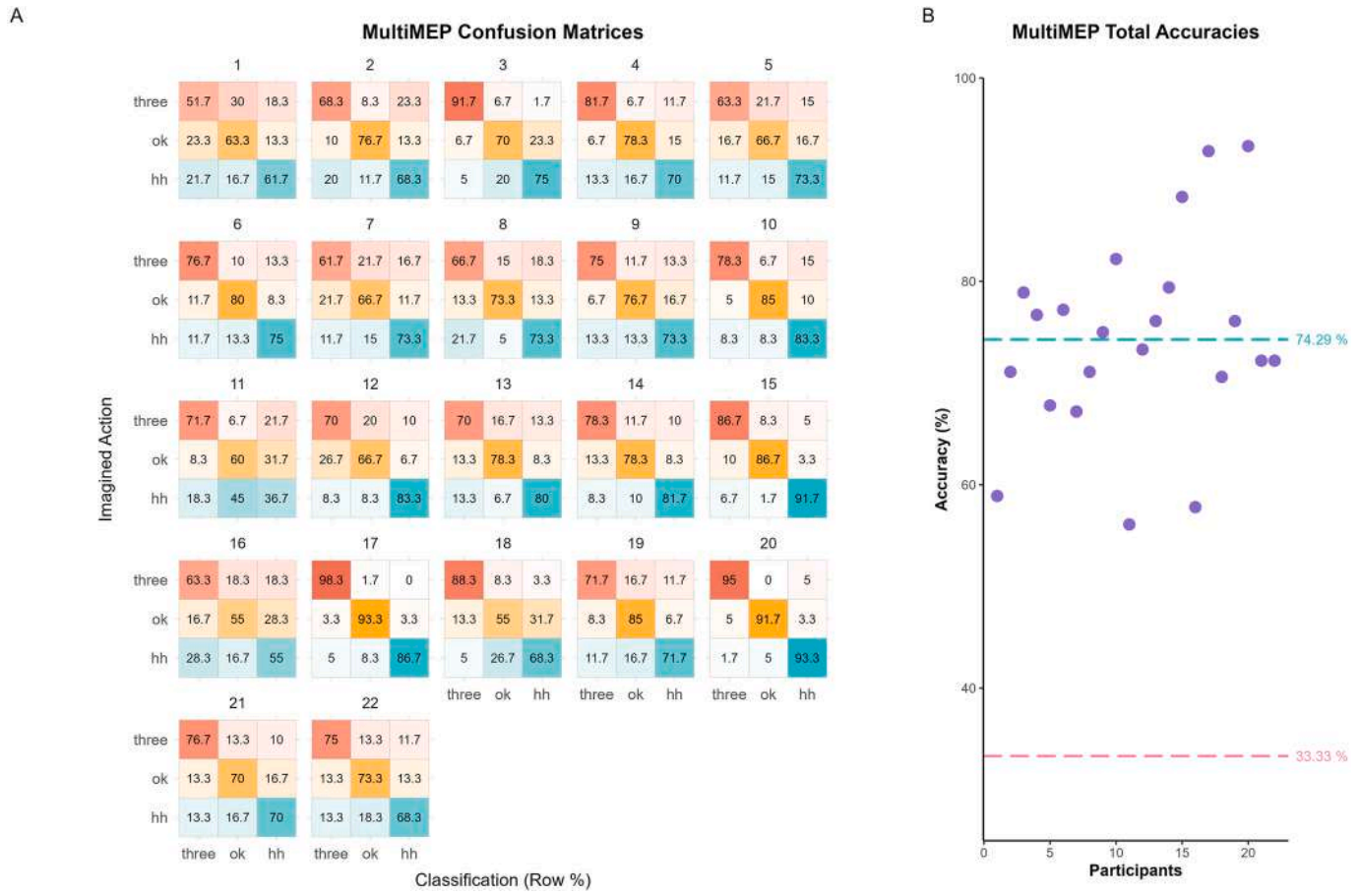

Fig. 6. MultiMEP Confusion Matrices and Total Accuracies

A. MultiMEP confusion matrices from each participant: within each imagined action category ("three" in red, "ok" in gold, "hitchhiking" (hh) in light blue), cells represent the % of trials predicted to belong to each of the three actions ("three", "ok" and "hh"). A perfect classification would highlight 100 % on the main diagonal cells and 0 % on the remaining cells of each row. Darker colors indicate better classification.

B. MultiMEP accuracies: each dot represents the classification total accuracy for each participant. The green dashed line represents the average total accuracy, while the pink one represents the theoretical chance level.

following [52], the likelihood that a 44.4 % classification accuracy is obtained by chance corresponds to a p-value <0.001, for a 41.6 % accuracy to $p < 0.01$, and for a 38.9 % accuracy to $p < 0.05$. Total accuracy was above 44.4 % for every participant ($p < 0.001$, Fig. 6).

Group total accuracy: We calculated if the average total accuracy among participants was higher than the theoretical chance level of 33.3 %. The average total accuracy was 74 % ± 10 % sd, significantly higher than the group chance level of 33.3 % ($W = 0$, $p < 0.001$, Fig. 6).

Classification Bias: We tested whether actions were classified with different accuracies across participants: no biases have been detected (Friedman $Q = 0.17$, $p = 0.91$; average accuracies: "three" = 75.5 % ± 11 % sd, "ok" = 74.1 % ± 10.5 % sd, "hh" = 73.3 % ± 12.0 % sd).

4.2. Exploratory analysis: cross-classification between contraction and imagery patterns

4.2.1. Sanity check: MultiEMG classification

MultiEMG classification showed an almost flawless total classification accuracy (98.7 % ± 0.01 % sd) with all participants above 44.4 % (Supplementary Materials Fig. S2).

4.2.2. MultiEMG-to-MultiMEP classification

The MultiEMG-to-MultiMEP classification was produced by training a classifier model on the MultiEMG data and then predicting MultiMEP imagined actions based on the hyperplanes estimated from the MultiMEG contraction patterns.

Single subject's total accuracy: The total classification accuracy was above 44.4 % ($p < 0.001$, Fig. 7) for 19 out of 22 participants, above 41.7 % for 20 out of 22 participants, and above 38.9 % ($p < 0.05$) for 21 out of 22 participants.

Group total accuracy: The average total accuracy was 54.3 % ± 11.2 % sd, significantly higher than the group chance level of 33.3 % ($W = 0$, $p < 0.001$, Fig. 7).

Classification Bias: Classification biases have been detected (Friedman $Q = 7.78$, $p = 0.02$), We employed three Wilcoxon tests to explore the differences in classification accuracy, comparing each combination of actions.

"three" vs. "ok": $W = 116.5$, $p = 0.75$, "three" (49.1 % ± 16.9 % sd), "ok" (51.5 % ± 17.5 % sd).

"three" vs. "hh": $W = 35.0$, $p = 0.005$, with "hh" (62.2 % ± 14.4 % sd) easier to classify than "three" (49.1 %±16.9 % sd).

"ok" vs. "hh": $W = 43.0$, $p = 0.02$, with "hh" (62.2 % ± 14.4 % sd) more easily classifiable than "ok" (51.5 % ± 17.5 % sd).

4.2.3. MultiMEP-to-MultiEMG classification

The MultiMEP-to-MultiEMG classification was produced by training a classifier model on the MultiMEP data and then predicting MultiEMG imagined actions based on the hyperplanes estimated from the MultiMEP patterns.

Single subject's total accuracy: The total classification accuracy was above 44.4 % ($p < 0.001$, Fig. 8) for all participants.

Group total accuracy: The average total accuracy was 71.7 % ± 13.1 % sd, significantly higher than the group chance level of 33.3 % ($W = 0$, $p < 0.001$, Fig. 8).

Classification Bias: No classification bias has been detected (Friedman $Q = 1.95$, p-value = 0.37).

4.3. Exploratory analysis: cross-subjects MultiMEP classification

Results revealed an average cross-subject classification accuracy of 41.9 % ± 4.33 % (Wilcoxon $W = 253$, $p < 0.001$) for the MultiMEP dataset. This indicates that, on average, a model trained on one participant's data was able to predict the imagined action from another participant's data nearly 42 times out of 100, suggesting a modest but

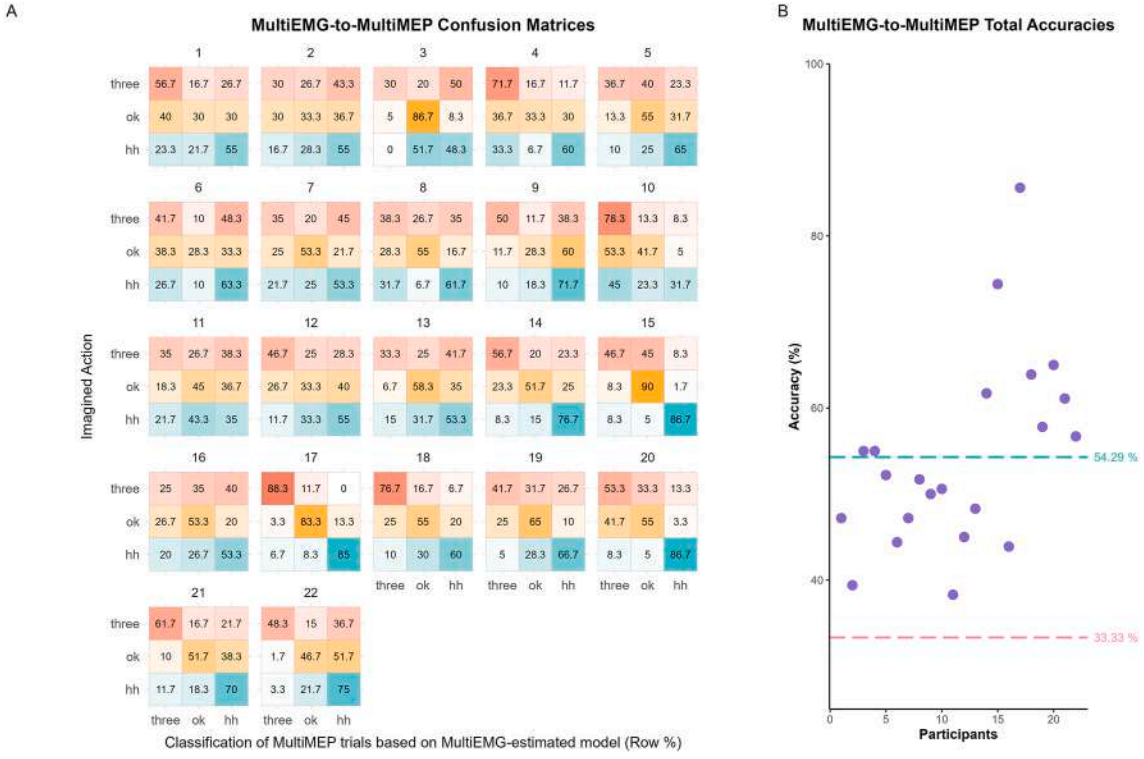

Fig. 7. MultiEMG-to-MultiMEP Confusion Matrices and Total Accuracies

A. MultiEMG-to-MultiMEP confusion matrices for each participant: rows represent the imagined action ("three" in red, "ok" in gold, "hitchhiking" (hh) in light blue). The cells constituting each row represent the % of trials predicted for the three action categories; differently from the MultiMEP analysis, the prediction model has been estimated using the MultiEMG patterns. **B.** MultiEMG-to-MultiMEP accuracies: each dot represents the classification total accuracy for each participant. The green dashed line represents the average total accuracy, and the pink one represents the theoretical chance level.

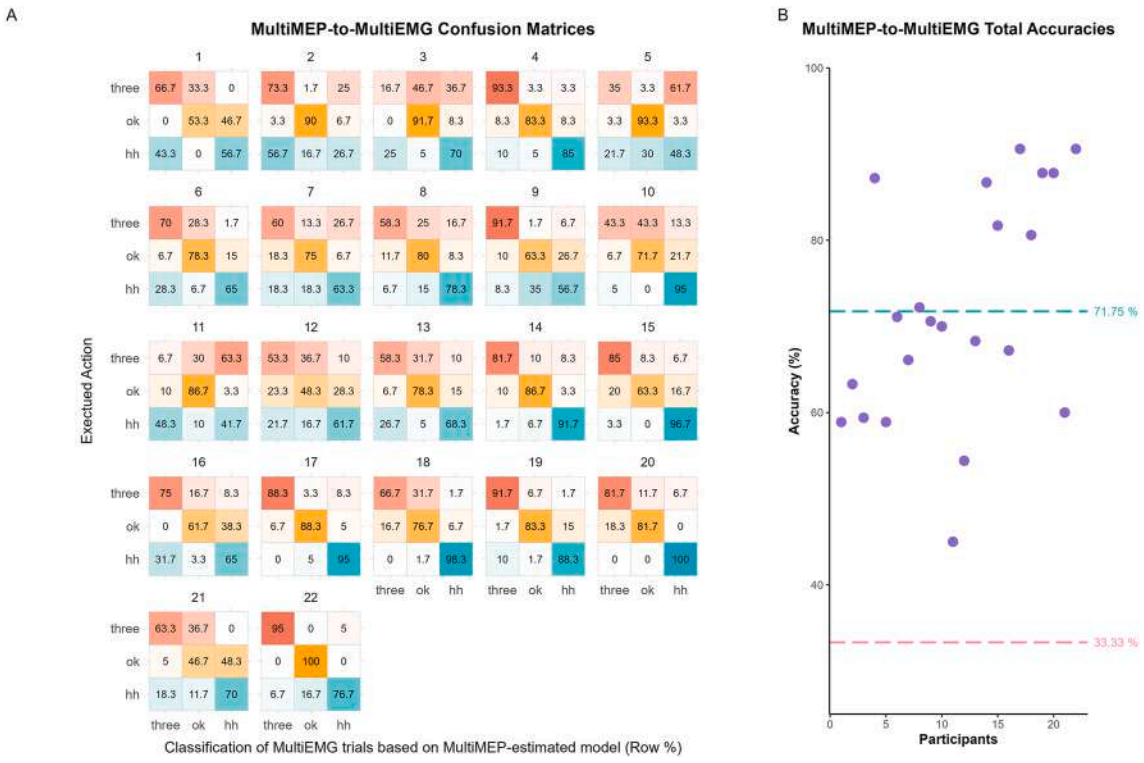

Fig. 8. MultiMEP-to-MultiEMG Confusion Matrices and Total Accuracies

A. MultiMEP-to-MultiEMG confusion matrices for each participant: rows represent the executed action ("three" in red, "ok" in gold, "hitchhiking" (hh) in light blue). The cells constituting each row represent the % of trials predicted for the three action categories; differently from the MultiMEP analysis, the prediction model has been tested on the MultiEMG patterns. **B.** MultiMEP-to-MultiEMG accuracies: each dot represents the classification total accuracy for each participant. The green dashed line represents the average total accuracy, and the pink one represents the theoretical chance level.

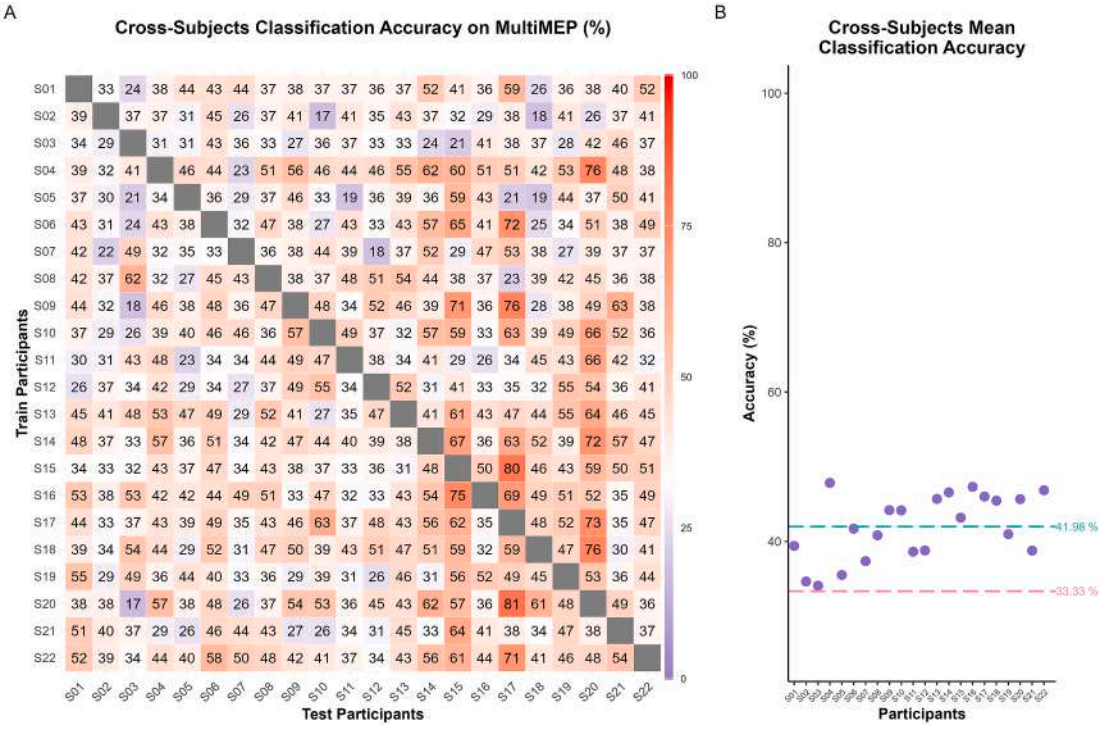

Fig. 9. Cross-Subjects Classification on MultiMEP

A. Cross-subjects confusion matrix: each cell indicates the classification accuracies obtained by training the classifier on the participant listed on each row and classifying on each remaining participant listed on the columns. A colorimetric scale is displayed with red indicating 100 %, dark blue 0 % and white 33 % accuracy. **B.** The plot displays the average classification accuracy for each participant.

reliable degree of similarity in decoding spaces across individuals (Fig. 9).

The same procedure applied to the MultiEMG dataset yielded a significantly higher cross-subject classification accuracy of 67 % ± 10 % ($W = 253$, $p < 0.001$), suggesting that overt action execution involves more consistent patterns of muscular activation across participants (Fig. 10).

These results suggest that participants partially share a common representational structure for imagining different actions. The relatively low classification accuracy likely reflects not only inter-subject variability in motor imagery, but also other factors that may have similarly impacted MultiEMG cross-subject classification. For instance factors such as the variability of the forarm sizes (the electrode spacing was fixed at 2.5 cm regardless of individual forearm anatomy), and slight variations in how participants executed the actions, could have affected the results. Such sources of variability may have limited the consistency of the recorded patterns across individuals.

4.4. *Exploratory analysis: MultiMEP classification accuracies for electrode grid subdivisions*

The Friedman-test applied to the 9 subdivisions indicates that these differ with respect to classification accuracies (Friedman $Q = 124.07$, $p < 0.001$; average accuracies on Table 1). The exploration of these differences by means of pairwise Wilcoxon tests indicates that, within each size subdivision, no forearm portion detects information better than other, i.e., on average all Quadrants pick similar information, and all Half-grids subdivisions pick similar information as well. The only consistent differences have been detected between grid sizes, as the Whole Grid classifies consistently better than each Half-grid subdivision, and each Quadrant. Similarly each Half-grid subdivision classifies better than each Quadrant (Fig. 11; see Figs. S3–S7 for more details).

Table 1
Average MultiMEP classification accuracy for electrode grid subdivisions.

	Subdivisions	Mean Classification Accuracy	SD
Quadrants	Dorsal Anterior	59.5 %	10.9 %
	Volar Anterior	60.3 %	10.3 %
	Dorsal Posterior	60.5 %	9.6 %
	Volar Posterior	58.9 %	10.7 %
Half-Grids	Anterior	69.9 %	10.4 %
	Posterior	69.2 %	9.7 %
	Volar	67.6 %	10.1 %
	Dorsal	69.2 %	11.1 %
Whole Grid		74.3 %	9.8 %

The table shows the mean classification accuracy percentage and the associated standard deviation for each subdivision.

5. Discussion

Design constraints in traditional 1m1a studies on covert motor processes limit the information retrievable from MEPs. In this proof-of-principle study, we adopted a decoding approach to multidimensional MEPs, achieving over 70 % classification accuracy for three complex imagined actions in all participants. This result suggests that single-trial MEP patterns carry more information than previously (implicitly) assumed.

Notably, we successfully classified actions involving different forearm muscles, broadening the potential of this technique to study covert motor processes for virtually any action. Expanding electrode coverage to the hand could further enhance accuracy. Once trained, the classifier enables single-trial classification of imagined actions, opening new research avenues. For example, MultiMEP can reveal the geometry of motor representations by analyzing how different covert motor processes are positioned in MultiMEP-space, akin to primate studies on action preparation and production [53–56].

Beyond distinguishing complex imagined actions, MultiMEP

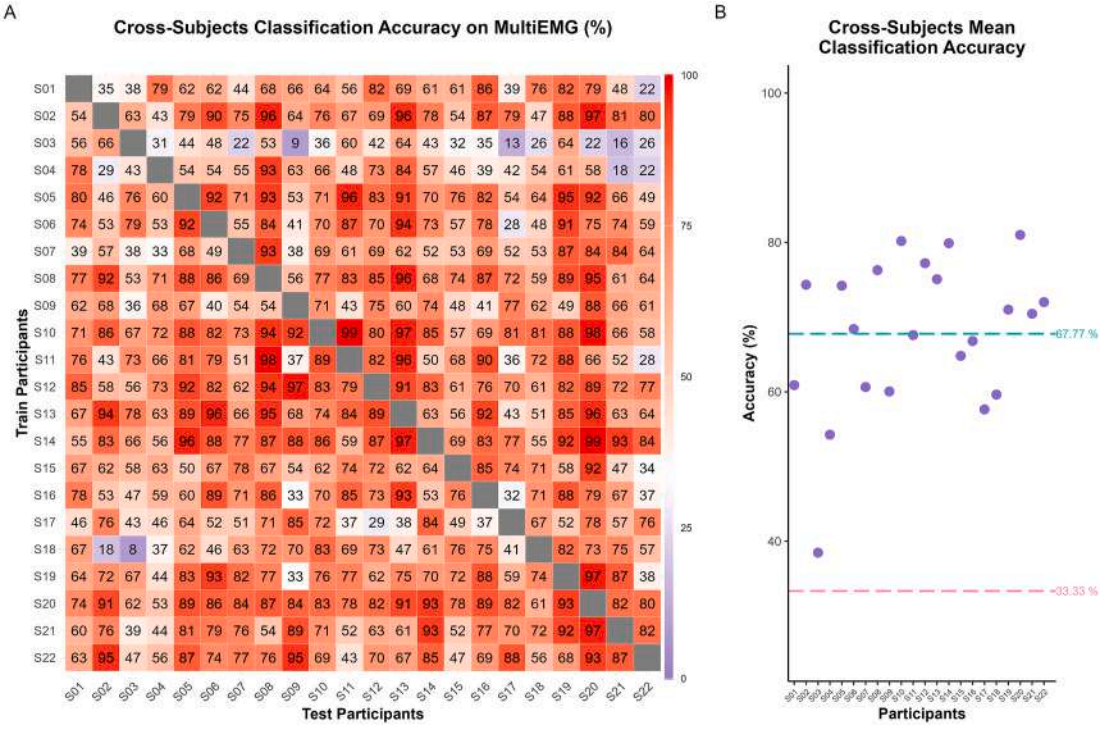

Fig. 10. Cross-Subjects Classification on MultiEMG
A. Cross-subjects confusion matrix: each cell indicates the classification accuracies obtained by training the classifier on the participant listed on each row and classifying on each remaining participant listed on the columns. A colorimetric scale is displayed with red indicating 100 %, dark blue 0 % and white 33 % accuracy. **B.** The plot displays the average classification accuracy for each participant.

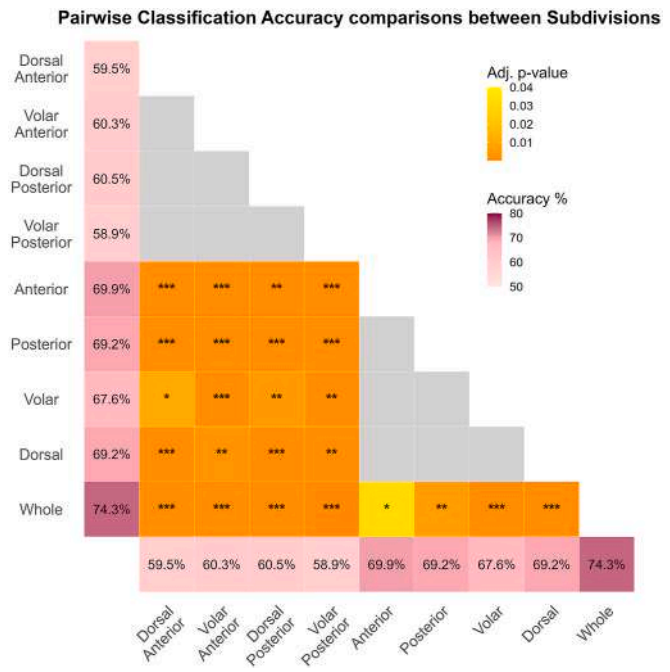

Fig. 11. Pairwise classification accuracy comparisons between subdivisions.

The figure shows the pairwise classification accuracy comparisons between all subdivisions. The first column and the last row (pink-shaded vectors) show the mean classification accuracy for each subdivision. The orange-shaded cells report significant p-value for each comparison ($p < 0.05$, Benjamini-Yekutieli corrected), while grey cells represent non-significant comparisons.

decoding allows inferences on the state of motor representations, much like 1m1a experiments. To test this, we computed contraction patterns for each action (MultiEMG) and compared them against MultiMEPs evoked during motor imagery. Our bidirectional cross-classification showed that hyperplanes estimated in one domain could discriminate classes in the other, in line with the claim that motor imagery and action production share the motor representations. However, despite being above chance in both directions, the analysis revealed an asymmetry: MultiEMG-to-MultiMEP achieved 54 % accuracy (with a positive bias in classifying "hh" actions), while MultiMEP-to-MultiEMG reached an accuracy of 71 %. This asymmetry likely reflects differences in the intrinsic discriminability of the two domains (classes within MultiEMG patterns being more separable than in MultiMEP), where classifiers trained on the more distinct dataset do not generalize well to the noisier one, despite a similar underlying structure. Following Van Den Hurk & Op De Beeck [57], we interpret the MultiMEP-to-MultiEMG results as a better reflection of the actual overlap between domains.

To explore whether motor imagery of the three actions produce similar patterns across participants we conducted a cross-subject classification analysis by training the classifier on each participant and testing its predictions on each remaining subject. This yielded a mean accuracy of 42 % for MultiMEP (motor imagery) and 67 % for MultiEMG. Although the MultiMEP performance was lower compared to other results in the present work, it was consistent across individuals and may reflect both individual differences in motor imagery and broader variability also evident in the MultiEMG classification. Factors such as fixed electrode spacing and subtle differences in action execution likely contributed to this variability, highlighting the need for future work to better control for anatomical and behavioral heterogeneity.

Eventually, we also explored the contribution of different forearm regions and the effect of grid size on classification performance. Across subjects, no single forearm portion consistently outperformed others in decoding imagined actions, likely because the muscles involved in each action spanned the entire grid. In contrast, grid size had a clear and consistent impact, with larger grids yielding higher classification accuracies. Notably, the improvement from Quadrants to the Whole Grid indicates a non-linear benefit, which suggests that our 24-electrode configuration may have approached a performance plateau.

In general, moving from a univariate to a multivariate datum allows to investigate problems from different perspectives, which might benefit the study of covert motor processes such as action observation or motor preparation. MultiMEP offers the possibility to study the processing of more ecological complex actions, adding generalizability to results, and putatively reducing the impact of sudden excitability shifts that decrease the signal-to-noise ratio, thus providing more stable outcomes. Most importantly though, it allows to explore different aspects of the datum that could not be captured through a 1m1a approach: for example, it has been shown that during motor preparation the corticospinal excitability inhibition precedes action execution [12]. Speculating, this inhibition might be accompanied to a certain degree by changes in cortical excitability patterns as well, which might clarify the different ways preparation affects selected, non-selected and irrelevant effectors [58]. Hypothetically, different stages of preparations might be discovered thanks to similarity analyses of MultiMEP pattern. Theoretically it might be possible to classify different covert motor states, such as imagery vs. preparation, and characterize their underlying multidimensional structures. MultiMEP decoding offers the possibility to study single-subject specific patterns in order to highlight the differences and the commonalities between participants. Eventually, single-trial characteristics should now represent a richer source of information: for example, is the variability of the MultiMEP pattern shape different throughout the delay period before imperative signals?

Although the fine-grained informational content recoverable through a MultiMEP approach remains to be fully understood, it would be worth investigating whether covert motor activities involving different motor contents and effectors (e.g., ipsilateral hand, feet, or mouth) are reflected in subtle or subthreshold pattern-specific modulations within the hand motor cortex. For instance, previous research has shown that preparing foot movements increases beta-band amplitude in the hand motor cortex [59]; it is possible that different feet actions preparation induce pattern-specific activities in the hand motor area. While such an outcome may seem counterintuitive, MultiMEP provides a unique opportunity to test similar possibilities and, importantly, to assess them in a subject-specific way. These are only a few open questions that we believe can be addressed when studying covert motor processes employing a MultiMEP setting.

Moreover, the MultiMEP setting can lead to different practical advantages. Notably, its putative increased sensitivity in detecting motor-related activity patterns may reduce the number of trials needed to detect condition differences, or, on the other hand, may allow the extraction of information-rich patterns that enhance effect sizes compared to traditional 1m1a approaches. The MultiMEP setting can also be used to inform new criteria for choosing stimulation hotspots. For instance, rather than relying on peak MEP amplitude from a single muscle, one could average MEP amplitudes across multiple electrodes to obtain a more stable estimate of general corticospinal excitability. Alternatively, hotspots could be defined based on non-standard criteria, such as maximal or minimal amplitude variability across electrodes, the presence of specific MultiMEP activation patterns, or any other metric computable on a data distribution. To enable such applications, information must be extracted online via an automated MultiMEP-Viewer. Integrating MultiMEP with real-time, automated state monitoring provides immediate feedback about the recorded physiological signal. For example, real-time MultiMEP settings might assist motor imagery training: in this scenario participants may imagine performing an action, while MultiMEP are evoked to assess the similarity between the imagery-induced state and the pattern shape associated to actual motor execution of the action.

Given the richness of MultiMEP data, it could be integrated into

other TMS protocols, including rTMS protocols [60,61], paired-pulse [62,63] and double-coil [64–67] paradigms, shifting from a unidimensional excitation/inhibition framework to a multidimensional perspective. Similarly, combining MultiMEP with TMS-evoked EEG activity could provide insight into how motor measures relate across the two different domains [68–71].

This paradigm shift may also benefit studies of pathological motor systems. Clinically, MEPs are used to assess corticospinal integrity [72,73], but offer little insight into cortical motor representations. MultiMEP could characterize motor system alterations with high granularity, extending its application to neuropsychiatric conditions where unidimensional MEP-derived measures are commonly used as biomarkers [74,75].

Compared to standard MVPA approaches in neuroimaging, MultiMEP offers key advantages. While fMRI and EEG-based Brain-Computer Interfaces achieve high classification accuracy (90–95 %) in tasks with well-separated motor representations (e.g., left vs. right-hand movements), they rarely explore finer effector-specific actions [36,76–80]. MultiMEP, by reflecting corticospinal states during covert motor tasks, extends motor system decoding from localized cortical patches to a physiologically meaningful space, mapping motor information onto hand and forearm muscles, where it can be more easily detected and discriminated. To evaluate MultiMEP potential as a Brain-Computer Interface, however, future studies must assess its test–retest reliability, with particular attention to how the latter is influenced by different tasks demands.

Finally, while the MultiMEP decoding framework differs methodologically from 1m1a experiments, the two forms do not represent a dichotomy. Intermediate strategies, such as decoding two-muscle setups, using unevenly spaced electrodes, or comparing averaged evoked patterns across conditions, can bridge the gap between traditional and multidimensional analyses, depending on the research question.

6. Conclusions

In summary, the MultiMEP decoding approach highlights the high discriminative power of MEP patterns at both single-subject and single-trial levels. Moreover, it extends to the inferential reach of 1m1a approaches while improving the generalizability of the results.

CRediT authorship contribution statement

Francesca Genovese: Writing – original draft, Visualization, Methodology, Investigation, Formal analysis, Data curation, Conceptualization. **Elena Mussini:** Writing – original draft, Visualization, Methodology, Investigation, Formal analysis, Data curation, Conceptualization. **Agnese Zazio:** Writing – original draft, Visualization, Conceptualization. **Fabio Beltrami:** Methodology, Investigation. **Marta Bortoletto:** Writing – original draft, Methodology. **Luigi Cattaneo:** Writing – original draft, Supervision. **Paolo Rota:** Validation, Supervision, Methodology. **Francesco Negro:** Writing – original draft, Supervision. **Martina Fanghella:** Writing – original draft, Visualization. **Corrado Sinigaglia:** Writing – original draft, Supervision, Resources. **Guido Barchiesi:** Writing – original draft, Visualization, Validation, Supervision, Software, Resources, Project administration, Methodology, Investigation, Funding acquisition, Formal analysis, Data curation, Conceptualization.

Funding

This work was supported by the PRIN grant [Title: Motor resonance during action planning and social interactions: from single neurons to brain circuits; CUP number: G53D23003190001; Code: 2022SP5K99_002] by the Italian Ministry of Education to G.B., by the PRIN grant [Title: The extended hand: psychophysical and neural foundations of a robotic supernumerary finger's use for grasping augmentation or recovery"; Code: 2022J72LFW_002] by the Italian Ministry of Education to C.S., and "Departments of Excellence 2023–2027" awarded to the Department of Philosophy of the University of Milan (G.B., C.S., E.M., F.G., M.F.); A.Z. was supported by the Italian Ministry of Health ('Ricerca Corrente').

Declaration of competing interest

The authors have nothing to declare.

Acknowledgements

We would like to thank Arianna Barchiesi for creating the stimuli displayed in the experimental session and Beatrice Fortunato for various visual materials.

Appendix A. Supplementary data

Supplementary data to this article can be found online at https://doi.org/10.1016/j.brs.2025.09.001.

References

[1] Fadiga L, et al. Corticospinal excitability is specifically modulated by motor imagery a magnetic stimulation study, vol. 37; 1998. p. 147–58.
[2] Grosprêtre S, Ruffino C, Lebon F. Motor imagery and cortico-spinal excitability: a review. Eur J Sport Sci 2016;16:317–24.
[3] Keogh R, Bergmann J, Pearson J. Cortical excitability controls the strength of mental imagery. eLife 2020;9:e50232.
[4] Meers R, Nuttall HE, Vogt S. Motor imagery alone drives corticospinal excitability during concurrent action observation and motor imagery. Cortex 2020;126:322–33.
[5] Ubaldi S, Barchiesi G, Cattaneo L. Bottom-Up and top-down visuomotor responses to action observation. Cerebr Cortex 2015;25:1032–41.
[6] Fadiga L, Fogassi L, Pavesi G, Rizzolatti G. Motor facilitation during action observation: a magnetic stimulation study. J Neurophysiol 1995;73:2608–11.
[7] Cattaneo L, Maule F, Barchiesi G, Rizzolatti G. The motor system resonates to the distal goal of observed actions: testing the inverse pliers paradigm in an ecological setting. Exp Brain Res 2013;231:37–49.
[8] Catmur C, Walsh V, Heyes C. Sensorimotor learning configures the human mirror system. Curr Biol 2007;17:1527–31.
[9] Craighero L, Zorzi V, Canto R, Franca M. Same kinematics but different objects during action observation: detection times and motor evoked potentials. Vis Cogn 2014;22:653–71.
[10] Naish KR, Houston-Price C, Bremner AJ, Holmes NP. Effects of action observation on corticospinal excitability: muscle specificity, direction, and timing of the mirror response. Neuropsychologia 2014;64:331–48.
[11] Derosiere G, Vassiliadis P, Duque J. Advanced TMS approaches to probe corticospinal excitability during action preparation. Neuroimage 2020;213:116746.
[12] Duque J, Lew D, Mazzocchio R, Olivier E, Ivry RB. Evidence for two concurrent inhibitory mechanisms during response preparation. J Neurosci 2010;30:3793–802.
[13] Duque J, Labruna L, Cazares C, Ivry RB. Dissociating the influence of response selection and task anticipation on corticospinal suppression during response preparation. Neuropsychologia 2014;65:287–96.
[14] Duque J, Ivry RB. Role of corticospinal suppression during motor preparation. Cerebr Cortex 2009;19:2013–24.
[15] Ficarella SC, Battelli L. Motor preparation for action inhibition: a review of single pulse TMS studies using the Go/NoGo paradigm. Front Psychol 2019;10:340.
[16] Hannah R, Cavanagh SE, Tremblay S, Simeoni S, Rothwell JC. Selective suppression of local interneuron circuits in human motor cortex contributes to movement preparation. J Neurosci 2018;38:1264–76.
[17] Tandonnet C, Garry MI, Summers JJ. Selective suppression of the incorrect response implementation in choice behavior assessed by transcranial magnetic stimulation: suppression of incorrect response implementation. Psychophysiology 2011;48:462–9.
[18] Aron AR, Verbruggen F. Stop the presses: dissociating a selective from a global mechanism for stopping. Psychol Sci 2008;19:1146–53.
[19] Claffey MP, Sheldon S, Stinear CM, Verbruggen F, Aron AR. Having a goal to stop action is associated with advance control of specific motor representations. Neuropsychologia 2010;48:541–8.
[20] Majid DSA, Cai W, George JS, Verbruggen F, Aron AR. Transcranial magnetic stimulation reveals dissociable mechanisms for global versus selective corticomotor suppression underlying the stopping of action. Cerebr Cortex 2012;22:363–71.
[21] Barchiesi G, et al. Sharing motor plans while acting jointly: a TMS study. Cortex 2022;151:224–39.

[22] Messina I, et al. Sex-specific automatic responses to infant cries: TMS reveals greater excitability in females than males in motor evoked potentials. Front Psychol 2016;6.
[23] Bestmann S, Krakauer JW. The uses and interpretations of the motor-evoked potential for understanding behaviour. Exp Brain Res 2015;233:679–89.
[24] Cattaneo L, Caruana F, Jezzini A, Rizzolatti G. Representation of goal and movements without overt motor behavior in the human motor cortex: a transcranial magnetic stimulation study. J Neurosci Off J Soc Neurosci 2009;29:11134–8.
[25] Cavallo A, Heyes C, Becchio C, Bird G, Catmur C. Timecourse of mirror and counter-mirror effects measured with transcranial magnetic stimulation. Soc Cognit Affect Neurosci 2014;9:1082–8.
[26] Fourkas AD, Avenanti A, Urgesi C, Aglioti SM. Corticospinal facilitation during first and third person imagery. Exp Brain Res Exp Hirnforsch Exp Cerebrale 2006;168:143–51.
[27] Naish KR, Obhi SS. Timing and specificity of early changes in motor excitability during movement observation. Exp Brain Res 2015;233:1867–74.
[28] Urgesi C, Candidi M, Fabbro F, Romani M, Aglioti SM. Motor facilitation during action observation: topographic mapping of the target muscle and influence of the onlooker's posture. Eur J Neurosci 2006;23:2522–30.
[29] Urgesi C, et al. Simulating the future of actions in the human corticospinal system. Cerebr Cortex 2010;20:2511–21.
[30] Haxby JV, Connolly AC, Guntupalli JS. Decoding neural representational spaces using multivariate pattern analysis. Annu Rev Neurosci 2014;37:435–56.
[31] Hebart MN, Baker CI. Deconstructing multivariate decoding for the study of brain function. Neuroimage 2018;180:4–18.
[32] Jimura K, Poldrack RA. Analyses of regional-average activation and multivoxel pattern information tell complementary stories. Neuropsychologia 2012;50:544–52.
[33] Weaverdyck ME, Lieberman MD, Parkinson C. Tools of the trade multivoxel pattern analysis in fMRI: a practical introduction for social and affective neuroscientists. Soc Cognit Affect Neurosci 2020;15:487–509.
[34] Rossi S, Pasqualetti P, Tecchio F, Pauri F, Rossini PM. Corticospinal excitability modulation during mental simulation of wrist movements in human subjects. Neurosci Lett 1998;243:147–51.
[35] Stinear CM, Byblow WD, Steyvers M, Levin O, Swinnen SP. Kinesthetic, but not visual, motor imagery modulates corticomotor excitability. Exp Brain Res 2006;168:157–64.
[36] Xygonakis I, Athanasiou A, Pandria N, Kugiumtzis D, Bamidis PD. Decoding motor imagery through common spatial pattern filters at the EEG source space. Comput Intell Neurosci 2018;2018:1–10.
[37] Rossi S, Hallett M, Rossini PM, Pascual-Leone A. Safety, ethical considerations, and application guidelines for the use of transcranial magnetic stimulation in clinical practice and research. Clin Neurophysiol 2009;120:2008–39.
[38] Rossi S, et al. Safety and recommendations for TMS use in healthy subjects and patient populations, with updates on training, ethical and regulatory issues: expert guidelines. Clin Neurophysiol 2021;132:269–306.
[39] World Medical Association. World medical association declaration of helsinki: ethical principles for medical research involving human subjects. JAMA 2013;310:2191–4.
[40] Merletti R, Cerone GL. Tutorial. Surface EMG detection, conditioning and pre-processing: best practices. J Electromyogr Kinesiol 2020;54:102440.
[41] Barchiesi G, et al. Head magnetomyography (hMMG): a novel approach to monitor face and whole head muscular activity. Psychophysiology 2020;57.
[42] Farina D, Mesin L, Martina S, Merletti R. Comparison of spatial filter selectivity in surface myoelectric signal detection: influence of the volume conductor model. Med Biol Eng Comput 2004;42:114–20.
[43] Guerrero FN, García PA, Spinelli EM. Signal modes for design-oriented analysis of active sEMG spatial filter electrodes. In: Torres I, Bustamante J, Sierra DA, editors. VII Latin American congress on biomedical engineering CLAIB 2016, bucaramanga, Santander, Colombia, October 26th -28th, 2016, vol. 60. Singapore: Springer Singapore; 2017. p. 504–7.
[44] Kothe C, et al. The lab streaming layer for synchronized multimodal recording. Imaging Neuroscience. https://doi.org/10.1162/IMAG.a.136; 2025. Advance Publication.
[45] Fukumoto Y, et al. Differences in motor imagery strategy change behavioral outcome. Sci Rep 2022;12:13868.
[46] Cattaneo L, Maule F, Tabarelli D, Brochier T, Barchiesi G. Online repetitive transcranial magnetic stimulation (TMS) to the parietal operculum disrupts haptic memory for grasping: Haptic working memory in the parietal operculum. Hum Brain Mapp 2015;36:4262–71.
[47] Maule Francesca, Barchiesi Guido, Brochier Thomas, Cattaneo Luigi. Haptic working memory for grasping: the role of the parietal operculum. Cerebral Cortex 2015 2015;25(2):528–37. https://doi.org/10.1093/cercor/bht252.
[48] Oostenveld R, Fries P, Maris E, Schoffelen J-M. FieldTrip: open source software for advanced analysis of MEG, EEG, and invasive electrophysiological data. Comput Intell Neurosci 2011;2011:1568–9.
[49] Pedregosa F, et al. Scikit-learn: machine learning in python. J Mach Learn Res 2011;12:2825–30.
[50] R Core Team. R: The R Project for Statistical Computing. https://www.r-project.org/. https://www.r-project.org/.
[51] Wickham H. Ggplot2. Springer Science+Business Media, LLC; 2016.
[52] Combrisson E, Jerbi K. Exceeding chance level by chance: the caveat of theoretical chance levels in brain signal classification and statistical assessment of decoding accuracy. J Neurosci Methods 2015;250:126–36.
[53] Elsayed GF, Lara AH, Kaufman MT, Churchland MM, Cunningham JP. Reorganization between preparatory and movement population responses in motor cortex. Nat Commun 2016;7:13239.
[54] Kaufman MT, Churchland MM, Shenoy KV. The roles of monkey M1 neuron classes in movement preparation and execution. J Neurophysiol 2013;110:817–25.
[55] Kaufman MT, Churchland MM, Ryu SI, Shenoy KV. Vacillation, indecision and hesitation in moment-by-moment decoding of monkey motor cortex. eLife 2015;4:e04677.
[56] Meirhaeghe N, Riehle A, Brochier T. Parallel movement planning is achieved via an optimal preparatory state in motor cortex. Cell Rep 2023;42:112136.
[57] Van Den Hurk J, Op De Beeck HP. Generalization asymmetry in multivariate cross-classification: when representation A generalizes better to representation B than B to A. Preprint at, https://doi.org/10.1101/592410; 2019.
[58] Bundt C, Huster RJ. Corticospinal excitability reductions during action preparation and action stopping in humans: different sides of the same inhibitory coin? Neuropsychologia 2024;195:108799.
[59] Pfurtscheller G, Neuper C, Andrew C, Edlinger G. Foot and hand area mu rhythms. Int J Psychophysiol 1997;26:121–35.
[60] Hamada M, Murase N, Hasan A, Balaratnam M, Rothwell JC. The role of interneuron networks in driving human motor cortical plasticity. Cerebr Cortex 2013;23:1593–605.
[61] Huang Y-Z, Edwards MJ, Rounis E, Bhatia KP, Rothwell JC. Theta burst stimulation of the human motor cortex. Neuron 2005;45:201–6.
[62] Coxon JP, Stinear CM, Byblow WD. Intracortical inhibition during volitional inhibition of prepared action. J Neurophysiol 2006;95:3371–83.
[63] Mrachacz-Kersting N, Stevenson AJT, Ziemann U. Short-interval intracortical inhibition and facilitation targeting upper and lower limb muscles. Sci Rep 2021;11:21993.
[64] Arai N, Lu M-K, Ugawa Y, Ziemann U. Effective connectivity between human supplementary motor area and primary motor cortex: a paired-coil TMS study. Exp Brain Res 2012;220:79–87.
[65] Cattaneo L, Barchiesi G. Transcranial magnetic mapping of the short-latency modulations of corticospinal activity from the ipsilateral hemisphere during rest. Front Neural Circ 2011;5.
[66] Davare M, Montague K, Olivier E, Rothwell JC, Lemon RN. Ventral premotor to primary motor cortical interactions during object-driven grasp in humans. Cortex 2009;45:1050–7.
[67] Davare M, Rothwell JC, Lemon RN. Causal connectivity between the human anterior intraparietal area and premotor cortex during grasp. Curr Biol 2010;20:176–81.
[68] Bortoletto M, et al. Asymmetric transcallosal conduction delay leads to finer bimanual coordination. Brain Stimul Basic Transl Clin Res Neuromodulation 2021;14:379–88.
[69] Guidali G, et al. Effects of transcranial magnetic stimulation (TMS) current direction and pulse waveform on cortico-cortical connectivity: a registered report TMS-EEG study. Eur J Neurosci 2023;58:3785–809.
[70] Zazio A, Barchiesi G, Ferrari C, Marcantoni E, Bortoletto M. M1-P15 as a cortical marker for transcallosal inhibition: a preregistered TMS-EEG study. Front Hum Neurosci 2022;16.
[71] Thong S, et al. Disinhibition across secondary motor cortical regions during motor sequence learning: a TMS-EEG study. J Neurosci 2025;45.
[72] Arora T, Desai N, Kirshblum S, Chen R. Utility of transcranial magnetic stimulation in the assessment of spinal cord injury: current status and future directions. Front Rehabil Sci 2022;3.
[73] Chen R, et al. The clinical diagnostic utility of transcranial magnetic stimulation: report of an IFCN committee. Clin Neurophysiol 2008;119:504–32.
[74] Kaskie RE, Ferrarelli F. Investigating the neurobiology of schizophrenia and other major psychiatric disorders with transcranial magnetic stimulation. Schizophr Res 2018;192:30–8.
[75] Vucic S, et al. Clinical diagnostic utility of transcranial magnetic stimulation in neurological disorders. Updated report of an IFCN committee. Clin Neurophysiol 2023;150:131–75.
[76] Ferracuti F, Iarlori S, Mansour Z, Monteriù A, Porcaro C. Comparing between different sets of preprocessing, classifiers, and channels selection techniques to optimise motor imagery pattern classification system from EEG pattern recognition. Brain Sci 2022;12:57.
[77] Khan RA, et al. A novel framework for classification of two-class motor imagery EEG signals using logistic regression classification algorithm. PLoS One 2023;18:e0276133.
[78] Lotte F, et al. A review of classification algorithms for EEG-based brain–computer interfaces: a 10 year update. J Neural Eng 2018;15:031005.
[79] Padfield N, Zabalza J, Zhao H, Masero V, Ren J. EEG-based brain-computer interfaces using motor-imagery: techniques and challenges. Sensors 2019;19:1423.
[80] Sharma R, Kim M, Gupta A. Motor imagery classification in brain-machine interface with machine learning algorithms: classical approach to multi-layer perceptron model. Biomed Signal Process Control 2022;71:103101.
[81] Barchiesi G, Cattaneo L. Early and late motor responses to action observation. Soc Cognit Affect Neurosci 2013;8:711–9.

[82] Classen J, Liepert J, Wise SP, Hallett M, Cohen LG. Rapid plasticity of human cortical movement representation induced by practice. J Neurophysiol 1998;79:1117–23.
[83] McMillan S, Ivry RB, Byblow WD. Corticomotor excitability during a choice-hand reaction time task. Exp Brain Res 2006;172:230–45.
[84] Ruffino C, Gaveau J, Papaxanthis C, Lebon F. An acute session of motor imagery training induces use-dependent plasticity. Sci Rep 2019;9:20002.
[85] D'Ausilio A, et al. Listening to speech recruits specific tongue motor synergies as revealed by transcranial magnetic stimulation and tissue-Doppler ultrasound imaging. Philos Trans R Soc B Biol Sci 2014;369:20130418.